to its length, hence the advantage of long tendons in ungulates (*11*). Sharks, and perhaps many bony fish, have their vast locomotory musculature entrained with the skin that acts as a whole-body tendon extending from the cranium to the tail end of the backbone.

If the shark's skin is to transmit forces of contracting muscles to the tail, the skin must be stiff for the duration of muscle contraction. Our findings lead us to the following interpretation: At rest, the muscles on both sides of the fish have the same length and cross-sectional area, and the fibers in the skin make a 60° angle with the fish's long axis. Internal pressure is low and so is skin stiffness.

To bend sharply as in fast swimming, the muscle on one side shortens and increases in cross-sectional area and girth. This causes fibers in the skin overlying the contracting muscles to increase their angle. The fiber angle controls the change in girth per unit change in length of the skin in concert with the surface of the contracting muscle. The changes in fiber angle imposed by the muscle causes the skin to remain taut in containing the muscle volume and to avoid wrinkling or loss of tension on the concave side of the fish.

Contracting muscle pulls on myosepta that pull on the skin and backbone. Since skin stiffness is high, tensile forces applied to it are transmitted by it from the head to the tail. Since the backbone resists compressive changes in the fish's body length, contracting muscles pull on one side of the head and tail causing the fish to bend rather than to shorten. The importance of the skin as an exotendon that transmits muscular force and displacement is, we believe, noteworthy.

S. A. WAINWRIGHT
F. VOSBURGH
J. H. HEBRANK
Zoology Department, Duke University, Durham, North Carolina 27706 and
Duke University Marine Laboratory, Beaufort, North Carolina 28516

References and Notes

1. We placed the point of a 19-gauge hypodermic needle attached to a Kulite semiconductor pressure transducer under the skin between the first and second dorsal fins half way between the lateral line and the middorsal septum. The lead was fixed to the first dorsal fin and led off to a Brush 220 chart recorder. The lead allowed the fish to resume its habitual swimming around the perimeter of a tank (8 m in diameter by 1.6 m depth) at Marineland, Inc., St. Augustine, Fla. All measurements of curvature and skin deformations were made from motion pictures taken with a Canon Scoopic 16-mm camera operated at 48 frames per second and analyzed with the aid of a Perceptoscope.
2. J. F. Daniel, *The Elasmobranch Fishes* (Univ. of California Press, Berkeley, 1928).
3. P. J. Motta, *Copeia* (1977), p. 454.
4. Six blacknose (*Carcharinus acronotus*), one dusky (*C. obscurus*), one spinner (*C. maculipinnis*), one sharpnose (*Rhizoprionodon terraenovae*), and one Florida smoothhound (*Mustelus norrisi*) were caught off Beaufort, N.C., and three lemon sharks were caught off St. Augustine, Fla. Pushing a sharp object to dent the lateral skin of a living or freshly dead shark causes two intersecting grooves to appear in the skin. These grooves radiate from the pressure point. We measured the azimuth of the grooves on the shark and, after having confirmed by dissection that the groove azimuth was the fiber azimuth on three sharks, we assumed all further groove azimuths to be fiber azimuths.
5. F. Vosburgh and J. H. Hebrank, in preparation.
6. S. A. Wainwright, W. D. Biggs, J. D. Currey, J. M. Gosline, *Mechanical Design in Organisms* (Arnold, Halsted, N.Y., 1976), pp. 180 and 293–298.
7. Stress in the skin = pr/t, where p = pressure, r = radius of cylinder, and t = skin thickness.
8. Samples were secured by snap swivels passing through holes in the sample edges. Wire fishing leaders connected the snap swivels to four sets of binding posts mounted 90° apart in the plane of the specimen. The use of point attachments permitted individual adjustment of tension in the wires and allowed stretch in the orthogonal direction. Two sets of binding posts were mounted to sliding carriages whose motions were controlled by lead screws and which caused extension of the sample. Extension in each direction was measured as the net movement between two pins stuck lightly in the sample. The pins drove the cores of colinear Linear Variable Differential Transducers. Force was held constant by monitoring sensor output and by adjusting the appropriate lead screw. Samples were bathed with fresh seawater during the experiments.
9. Skin deformation was metered by two thumbtacks stuck through a piece of flexible white plastic (0.5 mm thick by 15 mm wide by 80 to 150 mm long) into the skin of the shark. One tack held the skin and plastic in register while the other tack was attached to the skin but free to ride back and forth in a slot cut in the plastic. The length of the plastic and the distance between the tacks were measured on projected motion picture images, and the ratio of the intertack distance to length of plastic was computed for every fourth frame.
10. A. M. Gordon, A. F. Huxley, F. J. Julian, *J. Physiol. (London)* **184**, 170 (1966); B. C. Abbott and D. R. Wilkie, *ibid.* **120**, 214 (1953).
11. R. McN. Alexander and H. C. Bennet-Clark, *Nature (London)* **265**, 114 (1977).
12. We thank the staffs of the Duke University Marine Laboratory, the Cornelius Vanderbilt Whitney Laboratory of the University of Florida and Marineland, Inc., for services, hospitality, and unstinting cooperation. M. R. Hebrank gave vital assistance in every phase of the study. Prof. J. E. Gordon gave fruitful discussion and suggested we study torsion.

13 March 1978; revised 31 May 1978

Acoustic Detection of Cosmic-Ray Air Showers

Abstract. *The signal strength, bandwidth, and detection range of acoustic pulses generated by cosmic-ray air showers striking a water surface are calculated. These signals are strong enough to be audible to a submerged swimmer. The phenomena may be useful for studying very-high-energy cosmic rays and may help answer the important question of whether the origin of cosmic rays is extragalactic or galactic.*

Extensive air showers (EAS) created by cosmic rays with energies greater than 10^{19} eV (approximately 1 calorie) are predicted to occur with a frequency of 1.5×10^{-9} m^{-2} day^{-1} sr^{-1} (*1*). Obviously a large detector is required to observe these events with any regularity. I will show here that large bodies of water will convert this energy into a detectable acoustic signal and that these events are probably being detected, as undesired background noise by U.S. Navy fixed underwater acoustic installations used for the calibration of equipment and the measurement of underwater acoustic signals and spectra (*2*).

The source of cosmic-ray particles is an important unanswered question. Cosmic-ray protons with energies much greater than 10^{21} eV should not exist if their origin is extragalactic (*3*), since they lose energy through interactions with low-energy photons which constitute the 3°K universal background radiation. Events of this energy occur about 100 times less frequently than the 10^{19}-eV events. The largest instruments presently used will detect events above 10^{21} eV so rarely that their data will be inconclusive. The acoustic detection technique should determine the presence or absence of very-high-energy, cosmic-ray particles.

An EAS has three principal components (*3*). The first is the nuclear-active particle core containing about $^1/_8$ of the total energy in a radius of 10 m. The second is the electron component, with about the same fraction of the total energy as the nuclear component. Half of the electrons strike within a 50-m radius of the core. The third component, the muons, contain about $^3/_4$ of the total energy; one half of the muons strike within about 320 m of the core. The more energetic particles strike closer to the core. It

Table 1. Calculated detection range for an acoustic signal generated by the nuclear-active components of an EAS with energy $E_0 = 10^{19}$ eV.

Frequency	Sea state	Detection range (km)		
		0 dB	6 dB	20 dB
100 Hz	6	0.03	0.01	0.004
	0	0.2	0.1	0.02
1 kHz	6	0.02	0.01	0.004
	0	0.4	0.2	0.04
10 kHz	6	0.1	0.06	0.01
	0	2.0	1.2	0.3
30 kHz	6	0.3	0.2	0.04
	0	1.6	1.2	0.4
100 kHz	6	0.3	0.2	0.07
	0	0.5	0.4	0.2

0036-8075/78/1117-0749$00.50/0

Table 2. Estimated detection range (in kilometers), assuming that there are several values of E_0 and that the minimum detectable signal is 6 dB above sea state 0 noise.

E_0 (eV)	100 Hz	1 kHz	10 kHz	30 kHz
10^{17}	0	0.004	0.01	0.03
10^{18}	0.01	0.02	0.1	0.3
10^{19}	0.08	0.2	1.2	1.2
10^{20}	0.8	2	6	3
10^{21}	8	18	17	5
10^{22}	84	98	30	7

Table 3. Expected detection frequency of EAS by a single detector. The sensitive range is from Table 2. An acceptance angle of 2π steradians is assumed.

E_0 (eV)	Estimated event occurrence (km^{-2} day^{-1} sr^{-1})	Events expected per day by one detector			
		100 Hz	1 kHz	10 kHz	30 kHz
10^{17}	39	0	0.01	0.08	0.7
10^{18}	0.24	5×10^{-4}	2×10^{-3}	0.08	0.3
10^{19}	1.5×10^{-3}	2×10^{-4}	2×10^{-3}	0.04	0.04
10^{20}	10^{-5}	1×10^{-4}	8×10^{-4}	0.01	1×10^{-3}
10^{21}	6×10^{-7}	1×10^{-3}	4×10^{-3}	3×10^{-3}	3×10^{-4}
10^{22}	4×10^{-10}	6×10^{-5}	8×10^{-5}	7×10^{-6}	4×10^{-7}

has been demonstrated that both electromagnetic energy and energetic charged particles create acoustic pulses when impacting a fluid (*4*, *5*).

If the pressure associated with the acoustic pulse created by an extensive air shower striking a medium is estimated by assuming that the energy is deposited as thermal energy exponentially in our detection medium, then

$$E(x) = \frac{T(1 - e^{-\alpha x})E_0}{A}$$

where T is the fraction of energy that is transferred as thermal energy, E_0 is the energy in the shower, A is the area of the shower, and α is the attenuation length in the medium. The energy intensity will be

$$I = \frac{dE}{dt} = \frac{\alpha T e^{-\alpha x} E_0}{A}\frac{dx}{dt} = \frac{\alpha T c e^{-\alpha x} E_0}{A}$$

where c is the speed of light. The peak-to-peak pressure will be (*5*)

$$P = \frac{v \beta \alpha E_0 T c}{C_p J A}$$

where v is the velocity of sound in the medium, β is the volume coefficient of thermal expansion (*6*), C_p is the heat capacity at constant pressure, and J is the mechanical equivalent of heat.

A water target struck by the core particles depositing 1/8 of the total energy in 10-m radius will generate a pressure,

$$P = 8.5 \times 10^{-19} T E_0 \text{ dyne/cm}^2$$

where E_0 is measured in electron volts. Consider a specific example. Let $T = 1$ and $E_0 = 10^{19}$ eV: then the peak-to-peak pressure will be 8.5 dyne/cm^2 or 19 dB with reference to 1 dyne/cm^2 (93 dB with reference to 2×10^{-4} dyne/cm^2).

An underwater detector near the core of the shower would register a "click," whereas a detector far away would register something akin to thunder. (An observer close to a lightning strike hears a sharp crack, whereas a distant observer hears a low rumble.) The maximum detectable range depends upon the characteristic frequency of the sound and the background noise. However, the shifting to lower frequencies by the "thunder effect" should be beneficial since lower frequencies are significantly less attenuated in water.

It is believed (*6*) that pressure pulses of this magnitude are responsible for the "clicks" heard when a person's head is illuminated with pulsed microwave energy. A person in the core of an extensive air shower might also hear a "click" if the pulse is not too short. This would be a rare event, however, since only about one person in the world per year would happen to be in the core of a shower with energy greater than 10^{19} eV.

Calculation of the maximum detection range requires that the signal per frequency interval be compared to the noise in a similar frequency interval. The frequency bandwidth of the EAS-generated acoustic pulse is estimated by applying the uncertainty principle, $\Delta k\, \Delta(2R) \approx 1$, where k is 2π/wavelength and R is the radius of the particle impact area. The bandwidth is then $v/4\pi R$, and the signal pressure per 1-Hz bandwidth is

$$P_\nu = \frac{4\beta\alpha T c E_0}{C_p J R}$$

where ν is the frequency.

The 10^{19}-eV event will yield a pressure per 1-Hz bandwidth of 0.7 dyne/cm^2. This pulse will have a detection range as shown in Table 1. Noise and attenuation data are adapted from [(*7*), pp. 12–16]. Sea state 6 usually dominates over noise as a result of marine life and is therefore a measure of worse case background noise. Three signal-to-noise cases are listed, 0 dB where signal pressure is equal to equivalent noise pressure, 6 dB where signal pressure is twice the equivalent noise pressure, and 20 dB where signal is ten times the equivalent noise pressure. The detection range is frequency-dependent with a maximum between 10 and 30 kHz. Background noise cuts down the range at lower frequencies, whereas increased attentuation diminishes the range at higher frequencies.

In the calculations it is assumed that a spherical wave is propagating in infinitely deep seawater with constant temperature, salinity, and pressure. This assumption underestimates the range since channeling effects are prominent in the ocean.

Detection ranges for showers with various total energies are shown in Table 2. The more energetic showers exhibit a "bass boost" since they generate a low-frequency pulse that is much larger than the low-frequency noise. This low-frequency sound wave is essentially reduced in amplitude only by spherical spreading, whereas higher frequencies experience an additional attenuation as they travel. Thus, a large detectable range for showers with energy above 10^{19} eV is estimated. In Table 2 it is assumed that the minimum detectable signal occurs at 6 dB above sea state 0 noise. Tables 1 and 2 show that a single detector may have a sensitive detection radius of several kilometers for EAS with energies of 10^{19} eV or more.

The number of EAS events expected to be detected per day by a single detector are shown in Table 3. Each detector is assumed to have a sensitive radius as indicated in Table 2. Several events per week per detector are expected for EAS with primary energy at or below 10^{18} eV, if the detection frequency is 10 to 30 kHz. Higher-energy events would be detected at lower frequencies. The "thunder effect" should aid in the detection of these events. An array of 100 detectors would detect about three 10^{22} eV events per years at 1 kHz, if such events occur with the extrapolated frequency. Occurrence rates per EAS events with energy greater than 10^{19} eV are extrapolations from Andrews *et al.* (*1*) based on a slope of −2.2 with energy.

The human ear can easily detect acoustic signals 20 dB above the noise levels considered here [(*7*), p. 17]. Attenuation drops the signal below this level in a short distance; however, a diver should hear a "click" from a 10^{17}-eV EAS every week or so.

Actual signal detection ranges may well be larger than calculated here, since several mechanisms will tend to enhance them. These include concentration of the more energetic particles toward the core of the shower, channeling effects in the water, and correlation detection techniques. Each 6-dB (0.3 dyne/cm^2) increase in signal will increase the detected EAS events by approximately a factor of 4.

The contribution to the acoustic signature of an EAS by the various particles in the shower should be different, since they differ in this radial distribution from the core, total energy, and radiation absorption length. The strongest signal will come from the small region near the core where the nuclear particles strike. The electrons will contribute a weaker signal from a larger surface area, whereas the muons will contribute a similar signal whose origin is a larger surface area and a thicker layer because of their reduced interaction with matter. The muon energy distribution is peaked near the core, even though the particles are widely distributed.

The use of detectors with angular sensitivity should make it possible to pinpoint the position and area of the shower and thus the energy of the primary cosmic-ray particle. The spectral content and the radial distribution of sound generated at various distances from the core may allow one to obtain detailed information about the particles in the shower.

As stated earlier, the U.S. Navy has several sophisticated hydrophone listening stations that have operated for extensive periods of time. These stations have probably detected signals from EAS. The signals should appear as a broadband "rumbling" noise of moderate duration, with occasional short higher-frequency "clicks."

W. LOUIS BARRETT
*Physics Department,
Western Washington University,
Bellingham 98225*

References and Notes

1. D. A. Andrews, D. M. Edge, A. C. Evans, R. J. O. Reid, R. M. Tennent, A. A. Watson, J. G. Wilson, A. M. Wray, *Proc. 12th Int. Conf. Cosmic Rays* **3**, 995 (1971).
2. W. F. Clifford, in *Present and Future Civil Uses of Underwater Sound* (National Academy of Sciences, Washington, D.C., 1970), pp. 112–129.
3. K. L. Greisen, *Annu. Rev. Nucl. Sci.* **10**, 63 (1960).
4. R. M. White, *J. Appl. Phys.* **34**, 3559 (1963); L. R. Sulak, paper presented at the Clyde L. Cowan Memorial Symposium on Long-Distance Neutrino Detection, Washington, D.C., 25 April 1978.
5. L. S. Gournay, *J. Acoust. Soc. Am.* **40**, 1322 (1966).
6. K. R. Foster and E. D. Finch, *Science* **185**, 256 (1974).
7. Report of the Committee on Underwater Telecommunication, National Research Council, in *Present and Future Civil Uses of Underwater Sound* (National Academy of Sciences, Washington, D.C., 1970).
8. I thank the faculty and staff of the Electrical Engineering Department of the University of Washington for their support during the preparation of this manuscript.

19 May 1978; revised 17 July 1978

Metastable Oxygen Emission Bands

Abstract. *Recombination of ground-state oxygen atoms populates six different bound electronic states of molecular oxygen. Of the six optical transitions expected between the three upper states at 4 to 4.5 electron volts and the two lowest states, five have been observed in the afterglow of a conventional helium-oxygen microwave discharge in both $^{16}O_2$ and $^{18}O_2$, three of them for the first time in gas-phase spectra. Generation of these emissions from oxygen atoms in a system free of molecular oxygen establishes that atom recombination is the production mechanism.*

The spectroscopy of O_2 has been studied for the better part of a century (*1*, *2*), but a great deal still remains to be learned. Of particular importance in atmospheric chemistry are the six bound electronic states of O_2 which can arise from recombination of ground-state O atoms. The kinetic processes of production, radiation, and relaxation of these states are only now beginning to be understood. The relevant calculated potential energy curves are shown in Fig. 1 (*3*).

A peculiarity of O_2 is that all of these states are optically metastable with respect to each other; that is, the emission of radiation between any two states is a very slow process compared to the collisional mechanisms by which the excited molecule may lose its electronic energy. Typical radiative lifetimes for allowed electronic transitions are $\approx 10^{-8}$ second, whereas the average times required for isolated $O_2(b^1\Sigma_g^+)$ and $O_2(a^1\Delta_g)$ molecules to emit a photon and relax to the $X^3\Sigma_g^-$ ground state are 12 and 3900 seconds, respectively (*4*). This reluctance of the excited molecules to radiate has limited observations of the three upper O_2 states, $A^3\Sigma_u^+$, $C^3\Delta_u$, and $c^1\Sigma_u^-$. For the same reason, these molecules represent a potential energy reservoir in systems containing atomic O and are thus of kinetic importance. All three states have been observed in absorption from the ground state, and the transitions are known (*2*) as the Herzberg I, III, and II systems, respectively. However, only the $A^3\Sigma_u^+ \rightarrow X^3\Sigma_g^-$ transition has been observed in emission (*5*), except for a very weak pair of bands observed by Degen (*6*), which he was able to rotationally analyze and ascribe to the $c^1\Sigma_u^- \rightarrow X^3\Sigma_g^-$ transition.

Table 1. Band intensities of the $C^3\Delta_{1u} \rightarrow a^1\Delta_g$ system.

Band	Observed peak wavelength (Å)	Observed relative intensity	Calculated relative intensity
0–3	4553	0.03	0.07
0–4	4863	0.22	0.23
0–5	5212	0.58	0.49
0–6	5606	0.88	0.80
0–7	6055	1.00	1.00
0–8	6572	0.92	1.02
0–9	7172	0.59	0.83

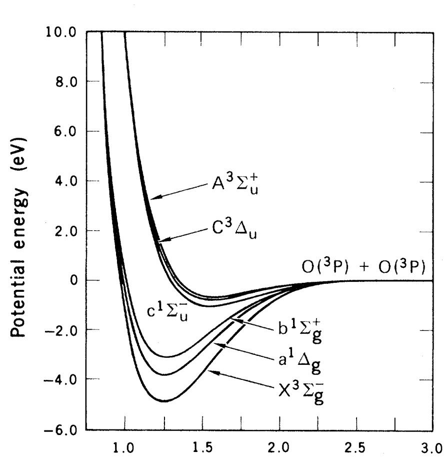

Fig. 1. Bound O_2 potential energy curves from the first dissociation limit (*3*).

When the Russian Venera 9 spacecraft sent back a spectrum of the dark side of Venus taken in the visible region (*7*), a very simple and intense spectrum of eight bands was observed, which was correctly identified by Lawrence *et al.* (*8*) as the 0–v'' progression of the $c^1\Sigma_u^- \rightarrow X^3\Sigma_g^-$ transition. This was a quite unexpected result, there being a very small amount of O_2 present in the venusian atmosphere as compared to the dominant gas, CO_2. Lawrence *et al.* then carried out laboratory experiments and were able to duplicate the Venus spectrum by passing a flowing He-O_2 mixture through a microwave discharge, adding CO_2 downstream and observing the resulting luminescence.

The mechanism of $c^1\Sigma_u^-$ formation was of considerable interest to me, particularly the question of the role of CO_2. The most obvious source of the $c^1\Sigma_u^-$ state is O atom recombination, yet, if the state is seen only in systems containing CO_2, a more complex mechanism must be postulated.

To learn more about c-X bands, I set up a conventional flowing afterglow apparatus and was soon able to duplicate the results of Lawrence *et al.*, obtaining intense c-X emission if I used a mixture of 30 mtorr O_2, 20 torr He, and 7 torr CO_2. Spectra were recorded photographically with a high-speed transmission grating image-tube spectrograph (*9*), with

0036-8075/78/1117-0751$00.50/0